Journal of Materials Chemistry A

ROYAL SOCIETY OF CHEMISTRY

PAPER

View Article Online
View Journal | View Issue

Cite this: J. Mater. Chem. A, 2025, 13, 37544

Efficiency and energy consumption analysis of bipolar membrane electrodialysis for electrochemical CO_2 capture

Sara Vallejo-Castaño, *[a] Giordana Bianchi,[a] Qingdian Shu,[a] Elise Mathiasin,[a] Michel Saakes,[a] Hubertus V. M. Hamelers[ab] and Philipp Kuntke *[ab]

Bipolar membrane electrodialysis (BMED) is an electricity-driven technology that captures and purifies CO_2, but its efficiency remains poorly understood. This work quantified coulombic efficiency losses in BMED for carbon capture using a fully saturated (1 M $KHCO_3$) and a partially saturated KOH solvent. Fully saturated solutions required 50% less energy consumption than partially saturated solutions for CO_2 purification and solvent regeneration. The minimum specific energy consumption was 161.2 kJ per mol CO_2 (3.65 GJ per ton CO_2) at 100 A/m^2 and was limited by parasitic potassium transport across the bipolar membrane, resulting in low CO_2 desorption efficiency (<60%) at low current density. Additionally, incomplete CO_2 desorption represented up to 10% of efficiency losses in most of the conditions tested. BMED displayed 100% CO_2 desorption efficiency (mol CO_2 per mol e^-) and a specific energy consumption of 290.61 kJ per mol CO_2 (6.60 GJ per ton CO_2) at industrially relevant current densities (1000 A/m^2). This work presents a robust analytical framework to identify coulombic efficiency losses and identifies the cause for low CO_2 desorption efficiency at a wide range of current densities and operational conditions, providing unique insights into the transport mechanisms in BMED and unlocking new pathways to maximize technology performance.

Received 17th June 2025
Accepted 1st October 2025

DOI: 10.1039/d5ta04909a

rsc.li/materials-a

1. Introduction

In the last 12 months, the earth's average surface temperature was 1.5 °C above pre-industrial levels,[1,2] breaching for the first time the temperature limit set by the Paris Agreement in 2015. To mitigate climate change and reach carbon neutrality by 2050, electrochemically driven CO_2 capture has emerged as an alternative well aligned with electrification strategies and has demonstrated similar energy requirements compared to conventional temperature swing methods.[3,4]

Electrochemical approaches regenerate the absorption capacity of CO_2 capture solvents by modulating their redox state or the pH.[5] For example, electrochemical regeneration of organic redox-active molecules such as sodium (3,3′-(phenazine-2,3-diylbis(oxy))bis(propane-1-sulfo-nate)) (DSPZ) demonstrated specific energy consumption (SEC) of 61 kJ per mol CO_2 at 200 A/m^2 and 10% CO_2 concentrations.[6] Electrochemically mediated amine regeneration (EMAR) – where the oxidation state of Cu modulates CO_2 absorption in ethylenediamine[7,8] – showed 50 kJ per mol CO_2 SEC at 50 A/m^2. Despite the low energy consumptions reported, low stability of the organic absorbents in the presence of O_2 (in the case of DSPZ) or electrode stability (in the case of EMAR) still hinder upscaling.[8] Alternatively, CO_2 can be desorbed using pH gradients that shift carbon speciation in solution to release CO_2 in acidic conditions and regenerate the solvent in alkaline conditions.[9] Gradients of pH can be realized through water electrolysis, hydrogen oxidation and evolution reactions, or bipolar membranes. These systems operate at ambient temperature and atmospheric pressure with alkaline absorbents. Water electrolysis requires high voltages and typically produces a mixture of O_2 and CO_2, while electrodes for H_2 oxidation require platinum as a catalyst, a precious metal with low abundance on earth's crust. Bipolar membranes (BPM) can also generate pH gradients through water dissociation and without H_2 or O_2 evolution reactions and have been used to desorb CO_2 from enriched solvents. BPMs do not contain precious metals, are stable at a wide range of conditions, and are currently produced on a large scale, making them relevant for electrochemical carbon capture.[3,10–12]

While bipolar membrane electrodialysis (BMED) was originally developed after 1956 to regenerate acid and base from industrial wastewater, only in 2009 experimental evidence of CO_2 release from carbonate solutions was demonstrated for the first time using the technology.[12] Since then, several pilot-scale systems have demonstrated CO_2 capture from flue gas, the air,

[a]Wetsus, European Centre of Excellence for Sustainable Water Technology, Oostergoweg 9, Leeuwarden 8911 MA, The Netherlands. E-mail: sara.vallejocastano@wetsus.nl

[b]Environmental Technology, Wageningen University, Bornse Weilanden 9 9, Wageningen 6708WG, The Netherlands. E-mail: philipp.kuntke@wur.nl

and the ocean, using BMED.[3,13,14] The minimum SEC reported depends on the application of the technology, but even for the same solvent composition and similar current conditions, SEC can vary widely in literature (100 to 166 kJ per mol CO_2 below 100 A/m^2 with fully saturated carbon-rich solutions).[3,12] The main challenge of the technology is that this minimum SEC exceeds theoretical predictions (<100 kJ per mol CO_2)[13] and the minimum thermodynamic energy requirement for CO_2 separation (20 kJ per mol CO_2)[13] impacting the competitiveness of the process (*vs.* amine based thermal regeneration).[4] Thus, although BMED is one of the most developed electrochemically driven CO_2 capture method,[15] the techno-economic feasibility of BMED for CO_2 capture depends on its SEC, and therefore, understanding and improving its efficiency remains essential to make it a commercially viable alternative.

Our prior research on BMED used a partially saturated alkaline solvent (K_2CO_3) representative of post-combustion carbon capture and demonstrated that low carbon concentration in the solvent was the main cause for low CO_2 desorption efficiency and high SEC (achieving 387 kJ per mol CO_2 at 250 A/m^2).[10] However, additional coulombic efficiency losses were not clearly identified due to the strong influence of carbon saturation of the solvent on CO_2 desorption efficiency. In this work, we used a fully saturated alkaline solvent (1 M $KHCO_3$) as the best possible scenario to benchmark the SEC and quantify the coulombic efficiency of a continuous BMED system. The experimental work was compared with theoretical results from an equilibrium model and was substantiated with carbon mass balances and charge balances. This robust analytical framework allowed to quantify coulombic efficiency losses related to incomplete CO_2 desorption, non-ideal K^+ transport in BPMs, and non-ideal H^+ transport in CEMs. This work demonstrates the reason behind low CO_2 desorption efficiency at a wide range of current densities and operational conditions, providing unique insights into the potassium transport mechanisms that affect current efficiency in BMED.

2. Experimental

2.1. Experimental method

In the BMED system used, bipolar membranes (BPM) and cation exchange membranes (CEM) were stacked together to create alternating acidic and alkaline compartments and convert electric current into a pH swing. A schematic representation of the process is shown in Fig. 1. When a carbon-rich stream entered the acidic compartment, K^+ ions were transported through the CEMs in the direction of the cathode and were replaced by H^+ generated by the BPM. The resulting decrease in pH induced CO_2 gas desorption from the acidic stream. Thereafter, the solvent was circulated through the alkaline compartment, where the K^+ ions were transported across the CEMs and recombined with OH^- generated by the BPM to restore the alkalinity of the solvent. Fully saturated solutions (1 M $KHCO_3$ + 0.05 M K_2SO_4) were used as rich solvents in the experiments. This solution had a carbon loading ($\alpha = [C_t]/[K^+]$) of 1 corresponding to the maximum carbon content that a KOH solvent can contain, and therefore a representation of the best case scenario possible for the CO_2 absorption step.[16,17] Additionally, partially saturated solutions (0.2 M $KHCO_3$ + 0.4 M K_2CO_3 + 0.05 M K_2SO_4) with a carbon loading (α) of 0.6 were used to evaluate BMED performance under more realistic conditions.[17]

The flow rate of rich solvent entering the regeneration stack ($\dot{V}_{rich}$) was selected based on the potassium load ratio (L_{K^+}). The load ratio defines the ratio of applied electrical current to K^+ ions fed into the system and was calculated as

$$L_{K^+} = \frac{iA_m N}{[K^+]_{rich} \dot{V}_{rich} F} \quad (1)$$

where i is the applied current density (A/m^2), A_m is the active membrane area (0.01 m^2), N is the number of cell pairs, $[K^+]_{rich}$ is the molar concentration in the influent solution (1.1 M), $\dot{V}_{rich}$

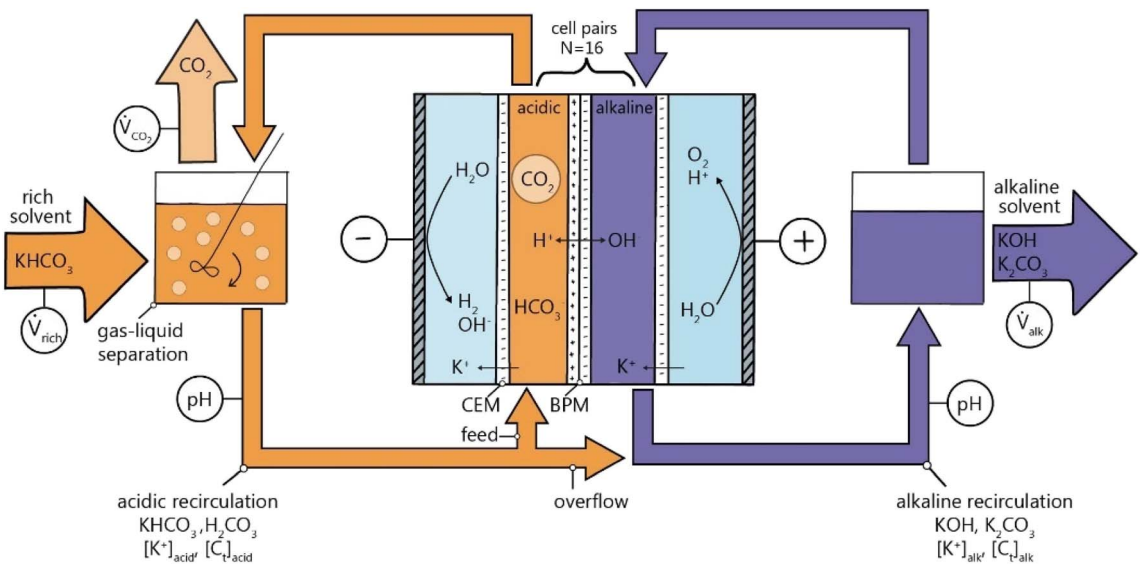

Fig. 1 Schematic representation of solvent regeneration and CO_2 desorption with BMED.

is the flow rate of the influent (L/s[1]), and F is the Faraday constant (96 485.3 C/mol).

Fully ($\alpha = 1$) and partially ($\alpha = 0.6$) saturated solutions were tested at a current density of 250 A/m^2, and L_{K^+} between 0.1 and 1.3. Thereafter, energy consumption and efficiency of fully saturated solutions were evaluated with two sets of experiments. First, experiments with fixed current density (100 A/m^2 and 250 A/m^2) with variable L_{K^+} of 0.1 to 1.2 were performed. Thereafter, experiments with fixed load ratio (0.7 and 0.9) and variable current density (50 to 1000 A/m^2) were carried out. One set of experiments (100 A/m^2 at variable L_{K^+}) was performed in duplicate to evaluate the variability of data. A detailed list of the tested parameters is shown in Table S1.

2.2. Materials

The system consisted of an electrochemical stack (EC, REDstack B.V, The Netherlands) with two PMMA end plates equipped with meshed platinized titanium electrodes (10 g Pt per m^2, 10 × 10 cm^2, Evoqua Water Technologies LLC/Magneto Special Anodes B.V., The Netherlands), with an active area of 10 cm × 10 cm. A 0.5 M (mol/L) K_2SO_4 electrode rinse solution was recirculated in the anode and cathode compartments to convert the electric current into an ionic current through oxygen and hydrogen evolution reactions, respectively. Between the electrodes, alternating BPM and CEM (Fumasep FBM, and Fumasep FKB-PK-130, Fumatech BWT GmbH, Germany) separated by polymeric spacer-gaskets of 480 μm thickness (Deukum, Germany) were used to create acidic and alkaline compartments. The stack was composed of 16 cell pairs, and each cell pair contained a BPM, a CEM, an acidic and an alkaline compartment, as shown in Fig. 1. The rich solvent influent was dosed using a Simdos® 10 liquid dosing pump (1 to 100 mL range). The acidic and alkaline streams were recirculated using a Cole-Parmer Masterflex L/S peristaltic pump at a flow rate of ∼650 mL/min to increase fluid velocity (∼1.3 cm/s) inside the stack. To operate in continuous mode, the flow rate of acidic solution entering the alkaline compartment (overflow) was equal to the rich influent stream, and alkaline flow rate exiting the stack ($\dot{V}_{rich} = \dot{V}_{alk}$). The CO_2 generated was separated using a continuously stirred flask at atmospheric pressure and measured using a CO_2 mass flow meter (Omega FMA-1607A Series, range 0.05–10 L/min, The Netherlands), the measured values were based on standard conditions of temperature and pressure (25 °C and 1.01 bar). The electric current was supplied by a Delta Elektronika SM3300 Series power supply (Germany). The voltage of the membrane stack was measured by subtracting the voltage of the gas evolution reactions from the total stack voltage using two Ag/AgCl reference electrodes (QM711X ProSense B.V., The Netherlands) placed at the anode and cathode sides. The pH of the acidic and alkaline compartments was measured using Memosens sensors (Endress + Hausser B.V., The Netherlands). The pH probes were calibrated prior to every experiment using pH standards of 4 and 10. All the experiments were performed until reaching a steady state. Process variables measured in line (current, reference electrodes voltage, CO_2 flow rate, and pH) were recorded on a data logger (RSG 40, Endress + Hauser B.V., The Netherlands). and analyzed to find the average values of all the measured variables during steady state. The rich, acidic and alkaline streams were sampled once the steady state was reached. The potassium concentrations were measured using ion chromatography (761 Compact IC, Metrohm, Switzerland) and the carbon concentrations were measured using total carbon analysis (TOC-L CPH, Shimadzu BENELUX, 's-Hertogenbosch, The Netherlands). A picture of the experimental setup used in this work is presented in Fig. S1 (SI).

2.3. Data analysis

2.3.1 Carbon balance. As illustrated in Fig. 1, the moles of carbon entering the system in the rich solvent are equivalent to the moles of CO_2 leaving in the gas phase, plus the remanent carbon dissolved in the regenerated alkaline solvent. Moreover, the solvent exiting the acidic and entering the alkaline compartment is always the same ($\dot{V}_{rich} = \dot{V}_{acid} = \dot{V}_{alk}$) implying that the carbon content of the streams must be equivalent. Hence, the carbon mole balance for the acidic and alkaline compartments can be written as:

$$\dot{V}_{rich}\left([C_t]_{rich} - [C_t]_{acid}\right) - \frac{\dot{m}_{CO_2,g}}{M_{CO_2}} = 0 \quad (2)$$

$$\dot{V}_{rich}\left([C_t]_{rich} - [C_t]_{alk}\right) - \frac{\dot{m}_{CO_2,g}}{M_{CO_2}} = 0 \quad (3)$$

where $\dot{V}_{rich}$ (L/s) is the volumetric flow rate of the rich stream, $[C_t]_j$ (mol C_t per L solution) is the total carbon concentration in stream j, with j = rich, acidic, or alkaline; $\dot{m}_{CO_2}$ (g/s) is the mass flow rate of CO_2 as measured in the gas stream, and M_{CO_2} is the molar mass of CO_2 (44.01 g per mol CO_2).

2.3.2 Key performance indicators. For an ideal system, every electron transported through the external circuit corresponds to one molecule of K^+ crossing the CEMs, and one molecule of H^+ and OH^- generated at the BPMs. Hence, CO_2 desorption can be related to electric charge through CO_2 production efficiency (η_{CO_2}). Which indicates the fraction of electrical current used to desorb CO_2 from the solvent and can be calculated for the gas stream as

$$\eta_{CO_2,gas} = \frac{\dot{n}_{CO_2}F}{iA_mN} \quad (4)$$

where F is the Faraday constant (F = 96 485.3 C per mol e$^-$), i is the current density (A/m^2), A_m is the active membrane area (A_m = 0.01 m^2), and N is the number of cell pairs (N = 16). Similarly, the CO_2 desorption efficiency can be calculated based on the difference in the carbon content between the rich stream, and the acidic, or alkaline streams as

$$\eta_{CO_2,acid} = \frac{\dot{V}_{rich}\left([C_t]_{rich} - [C_t]_{acid}\right)F}{iA_mN} \quad (5)$$

$$\eta_{CO_2,alk} = \frac{\dot{V}_{rich}\left([C_t]_{rich} - [C_t]_{alk}\right)F}{iA_mN} \quad (6)$$

When using a fully saturated solution ($KHCO_3$) where all the carbon entering the system is in the form of bicarbonate ions (HCO_3^-) every electric charge entering the system should result in the formation of one CO_2 gas molecule, as dictated by carbonate equilibrium reactions. Thus, the CO_2 desorption efficiency should be equal to 1 ($\eta_{CO_2} = 1$) when using a fully saturated solution. By the same token, for every electric charge entering the system, one K^+ is transported across each CEM to maintain overall charge neutrality. Therefore, another proxy for coulombic efficiency is the apparent transport number (t_{K^+}), which indicates how much of the current entering the system was used to transport potassium across the CEM from the acidic compartment to the alkaline compartment. The apparent transport number represents the observed potassium transport across multiple CEM and BPM cell pairs (N), and was calculated as

$$t_{K^+} = \frac{\dot{V}_{rich}([K^+]_{rich} - [K^+]_{acid})F}{iA_m N} \quad (7)$$

where $[K^+]_{rich}$ and $[K^+]_{acid}$ are the potassium concentrations (mol K^+ per L solution) in the rich and acidic streams, respectively. Moreover, the specific energy consumption SEC (GJ per ton CO_2) was calculated as

$$SEC = \frac{UiA_m}{\dot{n}_{CO_2}} \quad (8)$$

where U is the voltage across the membrane stack (V), calculated as $U = U_{ps} - U_{ref1} - U_{ref2}$ where U_{ps} is the voltage displayed on the power supply and U_{ref1} and U_{ref2} are the voltage measured by the two Ag/AgCl reference electrodes placed at the anode and cathode compartments. U excludes the voltage contribution of the electrode reactions. This correction was done under the assumption that the voltage of the electrode reactions is negligible compared to the stack voltage in large-scale stacks. The voltage per cell pair was calculated as the reference voltage divided by the number of cell pairs $U_{cell\ pair} = U/N$.

All the measured variables (concentrations, pH, CO_2 flow rate) and performance indicators (CO_2 desorption efficiency, energy consumption, *etc.*) were compared to a theory using the equilibrium model presented by Shu *et al.*, based on gas–liquid equilibria, transport and mass balances relations.[9]

3. Results and discussion

3.1. Fully saturated solutions provide more flexible operation

The effects of carbon loading in BMED were isolated from the effect of potassium concentration by varying the carbon concentration of the solvent while keeping a constant potassium concentration. Fig. 2 shows simulated and experimental results of (a) the desorption efficiency and (b) the specific energy consumption of fully and partially saturated solutions as a function of load ratio. Fig. 2(a) shows that increasing the carbon loading in the solvent enabled higher desorption efficiency across a wider range of load ratios, as indicated by the simulation lines. In contrast, partially saturated solutions

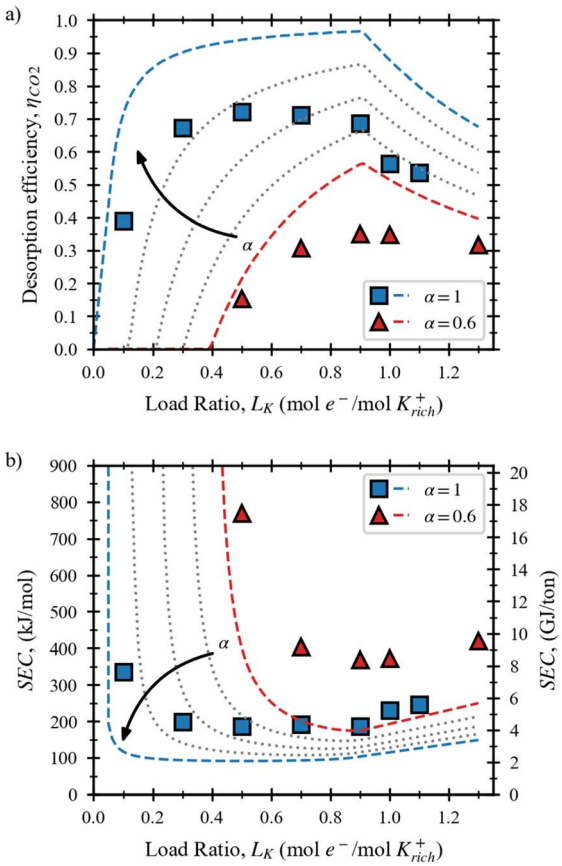

Fig. 2 (a) Desorption efficiency and (b) specific energy consumption of fully and partially saturated solutions as a function of load ratio at 250 A/m^2. Simulation results are lines and experimental data points are circles. Different colors used for different carbon loadings. Dashed lines indicate model results at intermediate carbon loadings α of 0.7, 0.8 and 0.9.

needed an initial energy investment to reach saturation before releasing CO_2. For example, while fully saturated solutions displayed high desorption efficiency (~90%) at a load ratio of 0.4, partially saturated solutions showed an efficiency of less than 20%. The latter requires that ~40% of the potassium ions are removed (and exchanged by H^+) before the solution starts releasing CO_2.

Furthermore, Fig. 2(a) shows that the CO_2 desorption efficiency increased proportionally to the carbon loading of the solvent. This was expected, considering that HCO_3^- ions require one H^+ while CO_3^{2-} ions require $2H^+$, to form carbonic acid (H_2CO_3). Nevertheless, the maximum CO_2 desorption efficiency (0.7) obtained with experiments at 250 A/m^2 was lower than expected.

The effects of improved desorption efficiency with fully saturated solutions were reflected in the specific energy consumption. Fig. 2(b) shows that the lowest energy consumption obtained at 250 A/m^2 was 4.2 GJ per ton CO_2, 50% lower than the SEC obtained for the partially saturated solution (8.4 GJ per ton CO_2), and in line with previous literature work.[9,16] This results highlight the importance of improving CO_2 absorption kinetic and thermodynamic limitations. The

following experiments were performed with fully saturated solutions because they represent the best-case scenario for a KOH solvent, serving as a benchmark electrochemical systems that do not consider CO_2 absorption limitations.

3.2. Efficiency and energy consumption at variable current density

The performance of BMED with fully saturated solutions at different current densities was tested at load ratios of 0.7 and 0.9. Fig. 3 shows experimental results of (a) the CO_2 desorption rate in mL_n per min, (b) the apparent transport number t_{K^+}, and (c) the CO_2 desorption efficiency $\eta_{CO_2,gas}$ as a function current density. Fig. 3(a) shows that the CO_2 desorption rate was directly proportional to the applied current density and matched the model predictions. However, Fig. 3(b) and (c) show that both CO_2 desorption efficiency $\eta_{CO_2,gas}$ and transport number t_{K^+} were lower than expected at low current densities. A decline in stack performance was observed at current densities below 250 A/m^2. Coulombic efficiency losses have been previously reported in BPM systems. Eisaman *et al.*, associated efficiency losses at low current densities to proton (H^+) leakage across ion exchange membranes[3] while Vallejo Castaño *et al.*, hypothesized that efficiency losses at low current densities stemmed from K^+ transport across the BPMs. Similarly, Parnamäe *et al.*, demonstrated with a theoretical model that the current is carried by ions – instead of protons and hydroxides – when operating BPMs below the limiting current density region (20 to 40 A/m^2).[18] Blommaert *et al.*, reported K^+ transport losses lower than 5% at a current density of 100 A/m^2,[19] while the present study found larger transport losses at the same current density. We hypothesize that differences in the solution composition and concentration on both sides of the BPM may explain the discrepancies with previous studies.

Fig. 4 shows (a) potassium concentration $[K^+]_{acid}$, and (b) pH in the acidic and alkaline compartments as a function of current density. Fig. 4 shows larger deviations – both in $[K^+]$, and pH – between measured values and model predictions at current densities below 250 A/m^2, supporting the previous findings on decreased efficiency. Moreover, Fig. 4(a) shows that while the model predicted a lower $[K^+]_{acid}$ at a load ratio of $L_{K^+} = 0.9$, the experiments showed similar concentrations between the two load ratios L_{K^+} tested. We hypothesize that larger concentration gradients arising at $L_{K^+} = 0.9$ augment non-ideal ion transport between acidic and alkaline compartments through the BPM or the CEM.

Fig. 5 shows (a) the cell pair voltage and (b) the specific energy consumption as a function of current density for experiments at load ratios of 0.7 and 0.9. Fig. 5(a) shows that the cell pair voltage at 50 A/m^2 was below the minimum voltage required for water splitting for a pH difference of 14 (0.829 V across the BPM).[9,20] First, this indicates that water splitting took place at voltages below the theoretical value of 0.829 V, but when combined with the findings from Fig. 3(c) it also shows that the process was not 100% efficient. Moreover, at high current density, the voltage was ~3 times larger than the theoretical voltage required for water splitting, indicating

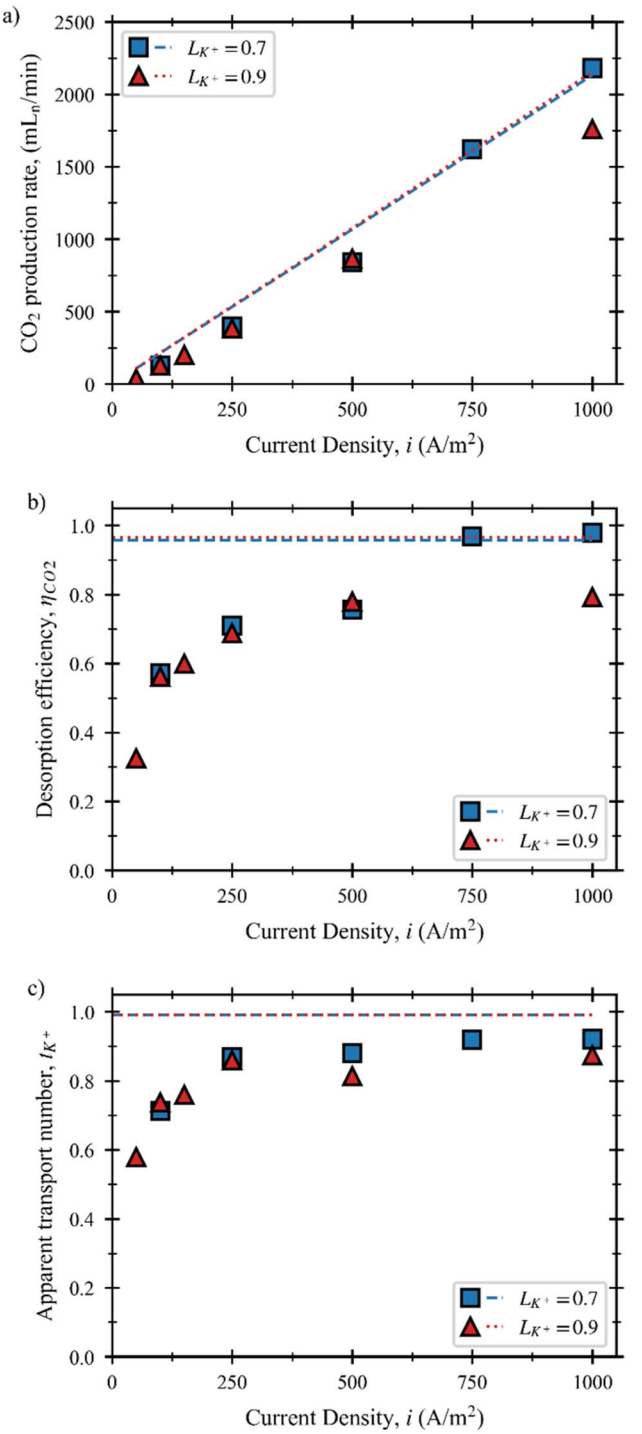

Fig. 3 Experimental results (symbols) and model predictions (lines) of (a) CO_2 desorption rate in mL_n per min, (b) CO_2 desorption efficiency $\eta_{CO_2,gas}$, and (c) apparent transport number t_{K^+} as a function current density for experiments at load ratios of 0.7 and 0.9.

additional resistances not accounted in the model. Fig. 4(b) shows that the minimum SEC achieved was 161 kJ per mol CO_2 (3.65 $GJ_{electric}$ per ton CO_2). This value is comparable to other values reported in literature for BMED[11] and to values reported for the thermal regeneration benchmark (monoethanolamine requires 3.6 $GJ_{thermal}$ per ton CO_2).[4,21,22] Nevertheless, it is

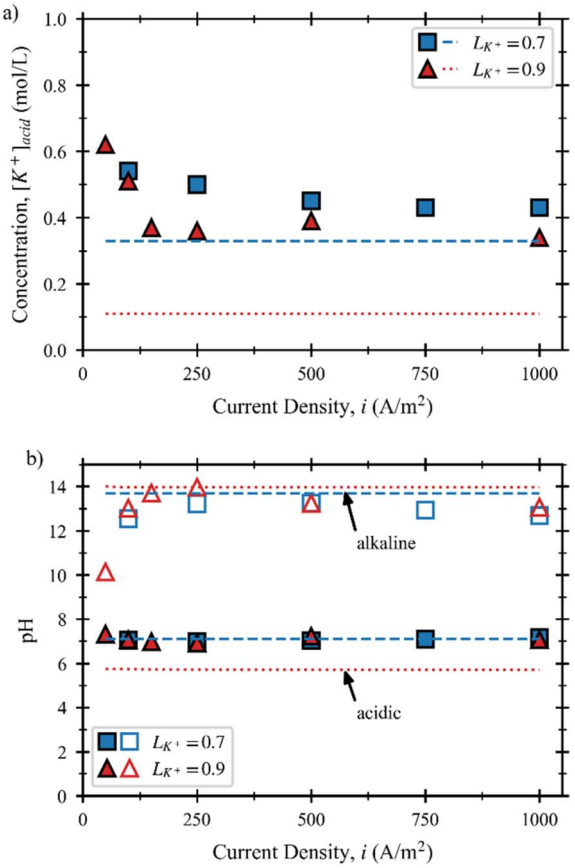

Fig. 4 Experimental results (symbols) and model predictions (lines) of (a) potassium concentration in mol/L, and (b) pH of the acidic and alkaline compartments as a function current density for experiments at load ratios of 0.7 and 0.9. Lines indicate model predictions for the measured variables.

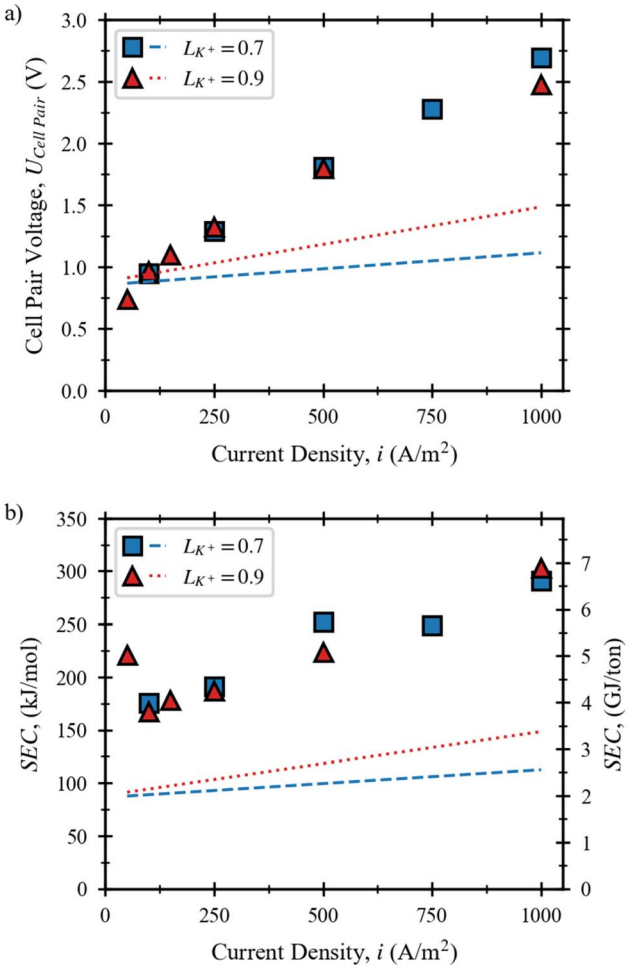

Fig. 5 Experimental results (symbols) and model predictions (lines) of (a) cell pair voltage, and (b) specific energy consumption as a function of current density for experiments at load ratios of 0.7 and 0.9.

important to note that electrical energy is equivalent to 2 to 3 times the magnitude of thermal energy.[23] Moreover, the MEA benchmark has been demonstrated for 90% CO_2 removal in integrated absorption/regeneration schemes, while in this case we evaluated an isolated regeneration system with a fully saturated solution. Shi *et al.*, demonstrated 90% CO_2 capture in a BMED system integrated with an absorption tower, however, the minimum energy consumption achieved was 5.8 GJ per ton CO_2 due to incomplete saturation of the solvent.[17] Therefore, strategies to maximize the carbon loading of the solvent should be implemented to achieve lower SEC in realistic conditions. The energy consumption obtained at 1000 A/m^2 was ~290.61 kJ per mol CO_2 (6.60 GJ per ton CO_2), comparable with the results of Eisaman *et al.* at the same current densities.[3] The results demonstrate that increasing current density from 100 to 1000 A/m^2 increased specific energy consumption by a factor of 2 while increasing desorption rates by a factor of 10. Hence, there is a clear benefit from working with BPMs at high current density, which arises from the non-linear BPM polarization behavior, highlighting the potential of BPMs for industrial applications where large rates of CO_2 absorption are required.

3.3. Efficiency and energy consumption at low current density

To further investigate efficiency losses at low current densities, subsequent experiments were performed at 100 and 250 A/m^2 while varying the load ratio from 0.1 to 1.2. Fig. 6 shows experimental results of (a) CO_2 desorption rate in mL$_n$ per min, (b) CO_2 desorption efficiency $\eta_{CO_2,gas}$, and (c) apparent transport number t_{K^+} as a function of load ratio. Higher load ratios correspond to lower flow rates of rich solvent treated. Fig. 6(a) and (b) confirmed substantially lower CO_2 production rates than model predictions at low current densities (100 and 250 A/m^2). Fig. 6(b) indicates that increasing the load ratio from 0.1 to 0.7, improved CO_2 desorption rate and efficiency, while at load ratios above $L_{K^+} = 0.7$ the performance improvements faded away. Overall, adjusting the load ratio to 0.7 allowed to maximize CO_2 desorption rate and efficiency.

Fig. 6(c) shows that transport numbers at 100 A/m^2 were lower than at 250 A/m^2, in line with the lower CO_2 desorption efficiency observed at lower current density in Fig. 6(b). Fig. 6(c) also shows that in most conditions the transport number was

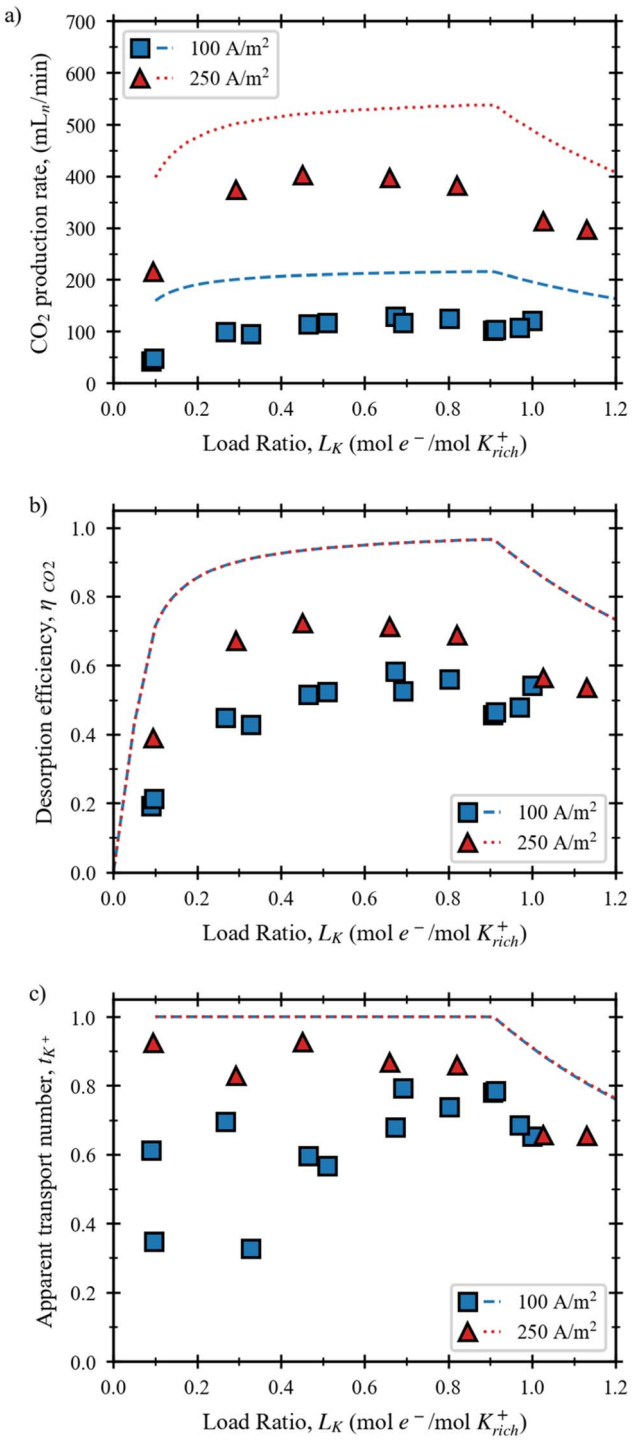

Fig. 6 Experimental results (symbols) and model predictions (lines) of (a) CO_2 desorption rate in mL_n per min, (b) CO_2 desorption efficiency $\eta_{CO_2,gas}$, and (c) apparent transport number t_{K^+} as a function of load ratio for experiments at current densities of 100 and 250 A/m^2.

substantially higher than the CO_2 desorption efficiency, which was unexpected. Moreover, at low load ratio ($L_{K^+} = 0.1$) 10% of the potassium ions in the rich solvent should be transported from acidic to alkaline compartment, leading to a theoretical CO_2 desorption efficiency of 0.6. In these conditions, if all the K^+ is transported effectively, the small amount of carbonic acid in solution limits CO_2 desorption efficiency. Since CO_2 desorption efficiency was always lower than expected, we hypothesize that slow desorption kinetics could limit CO_2 desorption efficiency.

Finally, the model in Fig. 6 shows that at load ratios larger than 1 ($L_{K^+} > 1$) a decline in CO_2 desorption is expected from the model. In this region, the applied current is more than enough to transport all the K^+ from acidic to alkaline compartment. Therefore, efficiency losses have been associated with H^+ transport across the CEM. Indeed, cation transport competition is expected when $[K^+]$ is low and $[H^+]$ is high in the acidic compartment.[9]

Fig. 7 shows (a) the $[K^+]_{acid}$ and (b) the pH of the acidic and alkaline compartments as a function of load ratio. Fig. 7 (a) shows that larger load ratios led to lower $[K^+]$ in the acidic compartment, but Fig. 7(b) shows that the pH was not lower than 6 and did not follow model predictions. This shows that $[K^+]$ was orders of magnitude larger than $[H^+]$ in the acidic compartment, indicating that H^+ transport across the CEM from acidic to alkaline compartment may not be the only source of efficiency loss. Another possible explanation is that at high load ratios, large concentration differences between acidic and

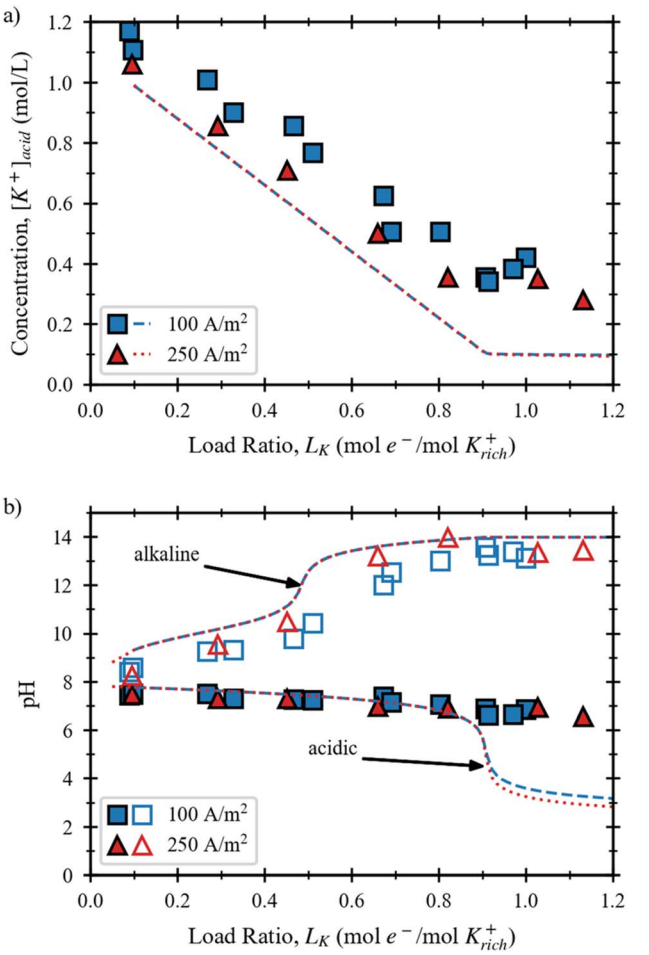

Fig. 7 Experimental results (symbols) and model predictions (lines) of (a) potassium concentration in mol/L, and (b) pH of the acidic and alkaline compartments as a function of load ratio for experiments at current densities of 100 and 250 A/m^2.

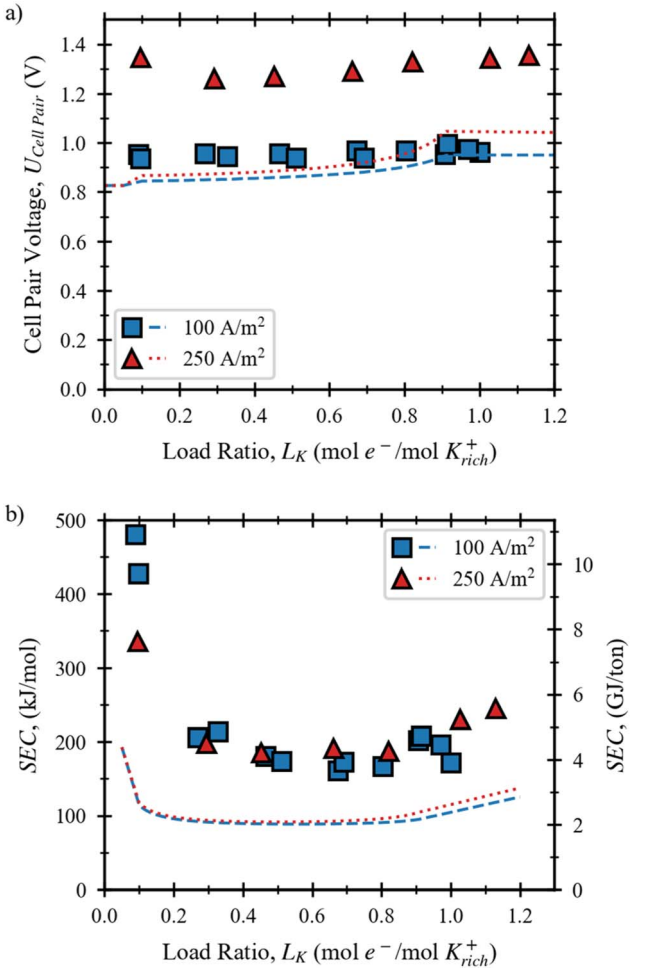

Fig. 8 Experimental results (symbols) and model predictions (lines) of (a) cell pair voltage, and (b) specific energy consumption as a function of load ratio for experiments at 100 and 250 A/m^2.

alkaline compartments enhance diffusive ion flux through the BPM or the CEM.

Finally, Fig. 8 shows (a) the cell pair voltage and (b) the specific energy consumption as a function of load ratio for experiments at current densities of 100 A/m^2 and 250 A/m^2. Fig. 8(a) shows that the influence of load ratio on cell pair voltage was negligible. Fig. 8(b) shows that the lowest energy consumption was 161 kJ per mol CO_2 (3.65 GJ per ton CO_2) obtained at 100 A/m^2 at a load ratio of 0.7. This energy consumption is comparable with other works in literature, and other electrochemical regeneration methods,[11,24] but it is still higher than the theoretical minimum.[13] Nevertheless, at low current density the voltage was close to the theoretical minimum. Therefore, the findings demonstrate that the minimum energy consumption was limited by coulombic efficiency losses rather than overpotentials in the BPM.

3.4. Potassium transport determines CO_2 desorption efficiency

The information was further analyzed to calculate deviations between experiments (exp) and model simulations (m) in the acidic compartment. These deviations in potassium $\Delta[K^+]_{acid}$- and carbon $\Delta[C_t]_{acid}$-concentrations were quantified as

$$\Delta[K^+]_{acid} = [K^+]_{acid,exp} - [K^+]_{acid,m} \quad (9)$$

$$\Delta[C_t]_{acid} = [C_t]_{acid,exp} - [C_t]_{acid,m} \quad (10)$$

where the theoretical concentration of potassium and carbon in the acidic compartment was calculated with an equilibrium model based on gas–liquid equilibria, transport and mass balance relations.[9]

Fig. 9 shows deviations ($\Delta[K^+]_{acid}$ and $\Delta[C_t]_{acid}$) for experiments at constant conditions of current density (a) 100 A m^{-2}, (b) 250 A m^{-2}, and load ratio (d) $L_{K^+} = 0.7$, (e) $L_{K^+} = 0.9$. Moreover, Fig. 9(a) and (b) show that deviations in potassium $\Delta[K^+]_{acid}$ and total carbon $\Delta[C_t]_{acid}$ were similar in magnitude, and were always lower at low load ratios. Fig. 9(d) and (e) show that $\Delta[K^+]_{acid}$ and $\Delta[C_t]_{acid}$ decreased with increasing current density, indicating better agreement between model and experimental results at high current density. Moreover, Fig. 9(e) shows that deviations $\Delta[K^+]_{acid}$ and $\Delta[C_t]_{acid}$ were larger at $L_{K^+} = 0.9$ than at $L_{K^+} = 0.7$. Larger deviations between experiments and model predictions at $L_{K^+} = 0.9$ could be attributed to concentration boundary layers, which may exacerbate local concentration gradients at the membranes surface.

Fig. 9 shows the deviations in carbon concentration $\Delta[C_t]_{acid}$ as a function of the deviations in potassium concentration $\Delta[K^+]_{acid}$ for experiments at (c) constant current density i, and (f) constant load ratio L_{K^+}. Fig. 9(c) and (f) display linearity between the deviations in potassium and total carbon concentration in the acidic compartment, demonstrating a correlation between these two variables. Fig. 9(c) shows that the deviations between experiments and model simulations were larger at 100 A/m^2 than at 250 A/m^2, while Fig. 9(f) also confirms larger deviations at $L_{K^+} = 0.9$ and at lower current densities. Thus, this analysis establishes a clear link between K^+ transport and carbon desorption efficiency in the acidic compartment.

3.5. Current efficiency losses identified from closing the carbon mass balance

To better understand performance losses, all the data collected was used to close the carbon balance and the charge balance for each experiment. Fig. 10 and 11 show the results for experiments at variable current density and variable load ratio, respectively. Fig. 10(a) and (d) show the total carbon concentration in the acidic, in the alkaline compartments, and the model predictions for experiments a $L_{K^+} = 0.7$, and $L_{K^+} = 0.9$, respectively. Fig. 10(a) shows that the theoretical and experimental results were in close agreement at load ratios of 0.7. In contrast, Fig. 10(d) shows that the predictions did not match experimentally measured carbon concentration at $L_{K^+} = 0.9$. Moreover, although the model predicted equivalent carbon concentration in both compartments, Fig. 10(a) and (d) show that carbon concentration in the alkaline compartment was always larger than in the acidic compartment. We hypothesize that the larger $[C_t]_{alk}$ measured may have been caused by incomplete CO_2 separation in the acidic stream caused by slow

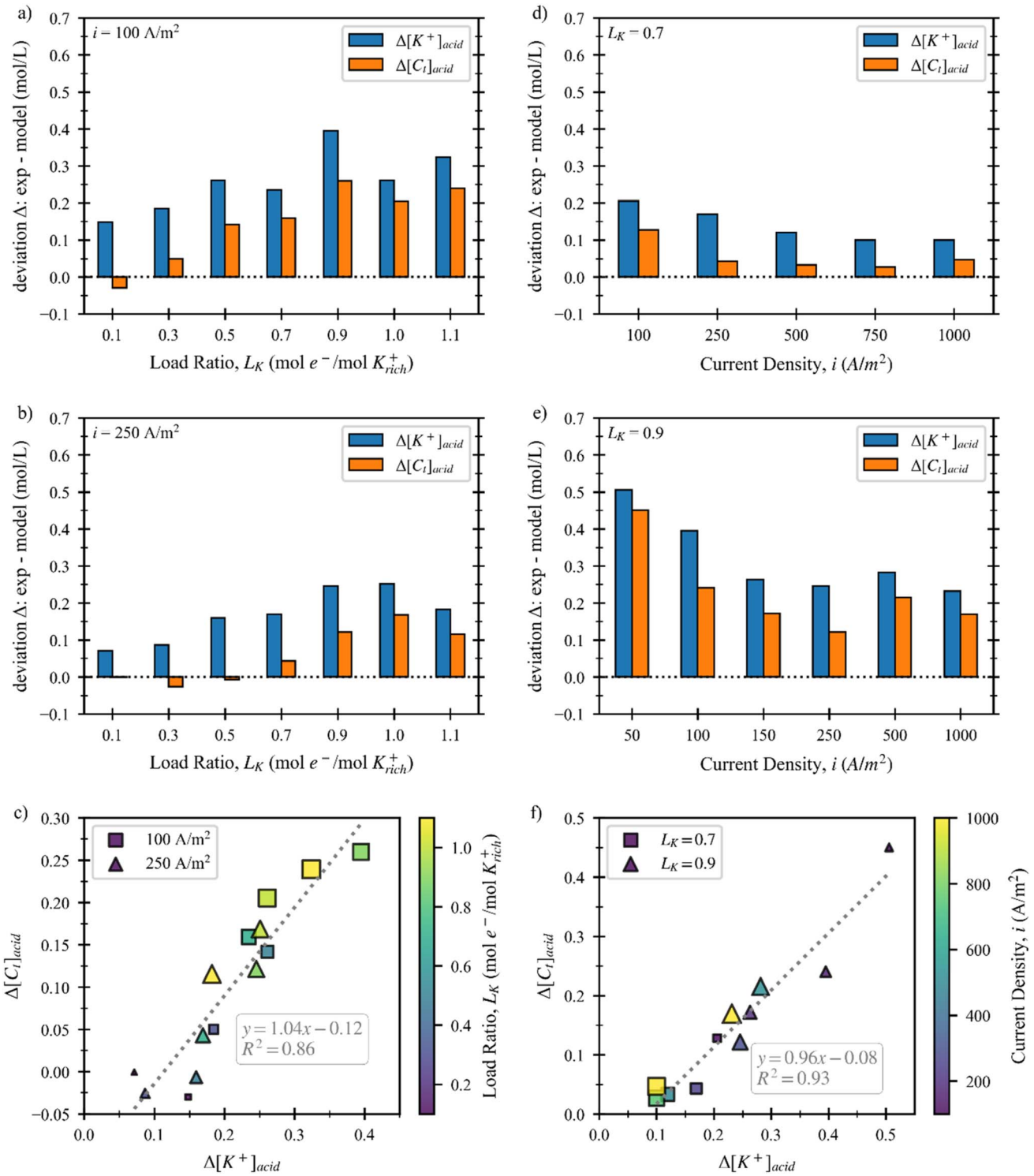

Fig. 9 Left column: differences between experimental and simulated potassium ($\Delta[K^+]_{acid}$) and carbon ($\Delta[C_t]_{acid}$) concentrations in the acidic compartment as function of load ratio for experiments at (a) 100 A/m^2, and (b) 250 A/m^2 (c) $\Delta[K^+]_{acid}$ *vs.* $\Delta[C_t]_{acid}$ for experiments at constant current density and variable load ratio (smaller and more transparent data points correspond to experiments at lower load ratios). Right column: Differences between experimental and simulated potassium ($\Delta[K^+]_{acid}$) and carbon ($\Delta[C_t]_{acid}$) concentrations in the acidic compartment as function of current density for experiments at (d) $L_{K^+} = 0.7$, and (e) $L_{K^+} = 0.9$. (f) $\Delta[K^+]_{acid}$ *vs.* $\Delta[C_t]_{acid}$ for experiments at constant load ratio and current density (smaller and more transparent data points correspond to experiments at lower current densities).

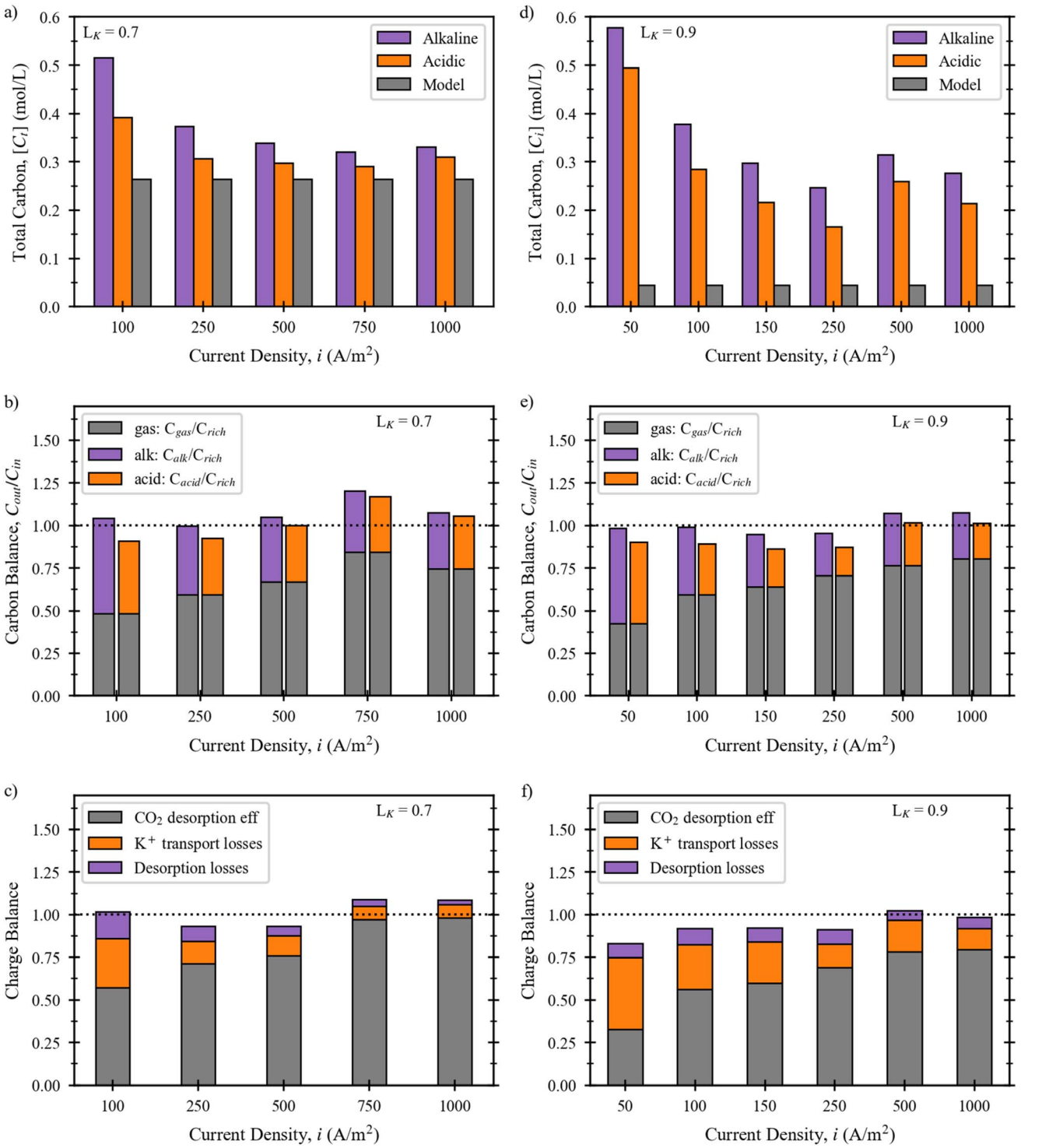

Fig. 10 Left column: results for experiments at a load ratio (L_{K^+}) of 0.7 and varible current density (i) – (a) total carbon concentration in acidic and alkaline compartments, (b) carbon mass balance for the acidic and the alkaline compartment, and (c) electric charge balance. Right column: results for experiments at a load ratio (L_{K^+}) of 0.9 and varible current density (i) – (d) total carbon concentration in acidic and alkaline compartments, (e) carbon mass balance for the acidic and the alkaline compartment, and (f) electric charge balance.

CO_2 desorption kinetics or by inaccuracies in TIC measurements.

Fig. 10(b) and (e) show the carbon balance for the acidic and the alkaline compartments at constant load ratios of (b) L_{K^+} = 0.7, and (e) L_{K^+} = 0.9. The carbon balance was performed by comparing the amount of carbon exiting the system through the liquid and the gas phase ($C_{\text{gas}} = \dot{m}_{CO_2,g}/M_{CO_2}$), to the total amount of carbon entering the system ($C_{\text{in}} = \dot{V}_{\text{rich}}[C_t]_{\text{rich}}$). The

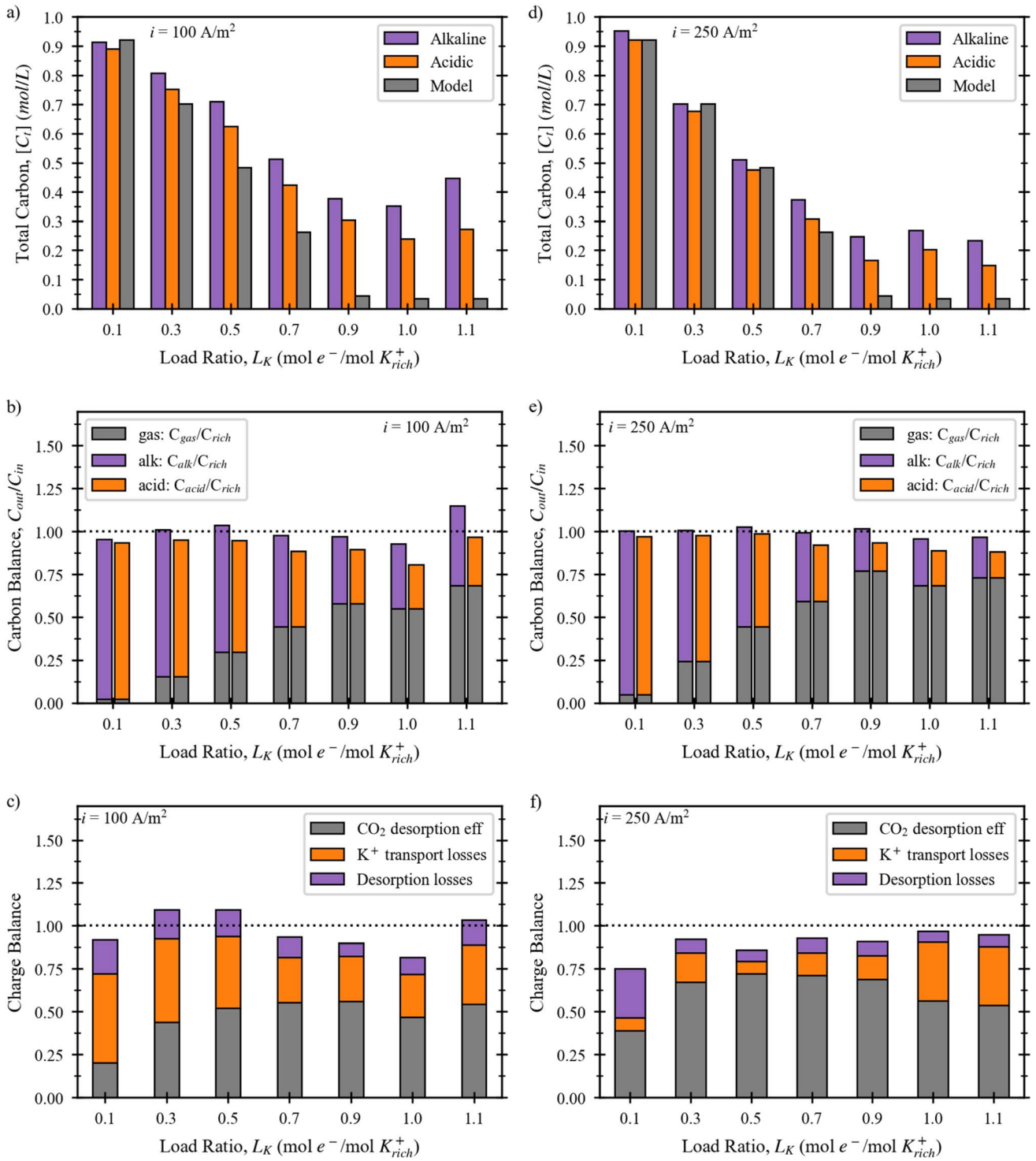

Fig. 11 Left column: results for experiments at a current density (i) of 100 A/m^2 and variable load ratio (L_{K^+}) – (a) total carbon concentration in acidic and alkaline compartments, (b) carbon mass balance for the acidic and the alkaline compartment, (c) and electric charge balance. Right column: results for experiments at a current density (i) of 250 A/m^2 and variable load ratio (L_{K^+}) – (d) total carbon concentration in acidic and alkaline compartments, (e) carbon mass balance for the acidic and the alkaline compartment, and (f) electric charge balance.

balance was performed independently for the acidic ($C_{\text{acid}} = \dot{V}_{\text{acid}}[C_t]_{\text{acid}}$) and the alkaline ($C_{\text{alk}} = \dot{V}_{\text{alk}}[C_t]_{\text{alk}}$) streams. These values were calculated by normalizing eqn (2) and (3) to the initial carbon content entering the system C_{in}. Out of 50 balances performed, only 10 closed with an error larger than 10%. Sources of error could come from small inaccuracies in sample analysis methods. Moreover, the absence of temperature control in the setup could have shifted the equilibrium towards more CO_2 production at high current densities. Additionally, inaccuracies in the CO_2 gas flow rate, may have affected

the results at high current density. Fig. 10(c) and (f) show the electric charge balance for experiments at $L_{K^+} = 0.7$, and $L_{K^+} = 0.9$, respectively. The contribution of each term to the charge balance was quantified as

$$\eta_{CO_2,gas} + (1 - t_{K^+}) + (\eta_{CO_2,acid} - \eta_{CO_2,alk}) = 1 \quad (11)$$

where the first term $\eta_{CO_2,gas}$ corresponds to the CO_2 desorption efficiency calculated from gas flow rate measurements. This term can also be interpreted as production of H^+ from the BPM which results in CO_2 desorption. The second term $(1 - t_{K^+})$ corresponds to an efficiency loss due to non-ideal potassium transport. The third term $(\eta_{CO_2,acid} - \eta_{CO_2,alk})$ accounts for the carbon concentration differences observed between alkaline and acidic compartments. As shown in Fig. 10(a) and (d) lower carbon concentrations were measured in the acidic samples than in the alkaline ones, while in theory both concentrations should be equal. We hypothesized that the carbonic acid generated did not evolve into CO_2 during the experiment due to slow CO_2 desorption kinetics and was redissolved and trapped in the alkaline stream as carbonate due to the high pH. Hence, enough K^+ was effectively removed and replaced by H^+ in the acidic compartment to form carbonic acid (H_2CO_3), but did not result in CO_2 desorption. Since the formation H_2CO_3 is an electric current investment, we concluded that this efficiency loss should be included in the charge balance.

By adding the three different terms described, we closed the charge balances with less than 10% error in 21 out of 25 experiments (86% of the experiments). The results demonstrate that the main sources of coulombic efficiency loss are incomplete CO_2 desorption, and non-ideal K^+ transport. Notably, Fig. 10(c) and (f) indicate that at low current density, CO_2 desorption efficiency decreased, and K^+ transport losses increased, demonstrating a direct link between K^+ transport losses and water dissociation in the BPM. This was confirmed with Fig. 11(c) and (f), which clearly show larger K^+ transport losses at 100 A/m^2 than at 250 A/m^2. Thus, we conclude that at low current density, water dissociation reactions are replaced by K^+ ion crossover through the BPM.[18,19,25]

From Fig. 11(a) and (c), experimental and modelled carbon concentration differences were more prominent at load ratios larger than 0.7. Contrary to theory, after reaching a load ratio of 0.9, the carbon concentrations in the alkaline compartment did not decrease further. Notably, although theory suggests that the optimum load ratio is 0.9, the data suggests the optimal load ratio was actually 0.7. At load ratios larger than 0.9, different losses are at play. Unwanted diffusive transport may result from large concentration and pH gradients between acidic and alkaline compartments. Moreover, transport competition between H^+ and K^+ across the CEM may result from low $[K^+]$ in the acidic compartment at higher load ratios. Since the BMED stack contained BPMs are CEMs, it was not possible to differentiate the contribution of each type of membrane to non-ideal K^+ transport. Other types of losses such as carbonate transport across the membranes, osmotic transport, or ionic shortcuts (occurring when many cell pairs are put together) were not evaluated either. Future fundamental transport studies on individual stack components level should quantify and identify all the sources of efficiency losses.

4. Conclusion

This work evaluated the performance of a BMED stack for continuous CO_2 purification and solvent regeneration. The minimum SEC was 161 kJ per mol CO_2 (3.65 GJ per ton CO_2) at 100 A/m^2 with a fully saturated solvent (1 M $KHCO_3$) and was 50% lower than that of a partially saturated solvent. The main limitation to achieve even lower specific energy consumptions was non-ideal transport of potassium across the BPM, limiting CO_2 desorption efficiency to less than 60%. This work highlights the impact of solvent composition and concentration gradients on BPM efficiency and emphasizes the need for more selective anion exchange layers in BPMs to minimize undesired ion crossover effects dominant at low current density.

The electric charge balance performed for all the conditions tested pinpointed to additional efficiency losses. Incomplete CO_2 separation from the acidic stream had a minor contribution (~10%) to CO_2 desorption efficiency, while H^+ transport across the CEM was a significant efficiency loss at a load ratio larger than 0.7. Further studies should evaluate the effect of large concentration gradients on individual stack components (BPMs and CEMs) under relevant operational conditions to obtain further insights.

At high current density (1000 A/m^2), BMED demonstrated a CO_2 desorption efficiency of 100%, and a specific energy consumption of 290.61 kJ per mol CO_2 (6.60 GJ per ton CO_2). Increasing current density from 100 A/m^2 to 1000 A/m^2 increased CO_2 desorption rates by a factor of 10, with a modest specific energy consumption increase of a factor of 2. This highlights the potential of BMED for industrial applications where large current densities, and rates of CO_2 absorption are required. This work provides a deep conceptual framework to understand the transport mechanisms that affect coulombic efficiency and limit the minimum energy consumption in BMED. These unique insights unlock new pathways to optimize the technology and to reach affordable Giga-ton scale CO_2 capture.

Author contributions

Sara Vallejo-Castaño: writing – original draft, conceptualisation, data curation, formal analysis, methodology, visualisation, writing – review & editing. Giordana Bianchi: investigation, formal analysis, writing original draft. Qingdian Shu: formal analysis, software, methodology. Elise Mathiasin: investigation. Michel Saakes: writing – review & editing. Hubertus V. M. Hamelers: conceptualisation, software, resources, methodology, supervision, writing – review & editing. Philipp Kuntke: conceptualisation, visualisation, software, data curation, writing – review & editing, supervision.

Conflicts of interest

There are no conflicts of interest to declare.

Data availability

The data supporting this article have been included as part of the supplementary information (SI). Supplementary information: (1) data tables reporting operational results for carbon loading of 0.6 and 1.0 at different load ratio and current densities, and (2) a photograph of the experimental setup. See DOI: **https://doi.org/10.1039/d5ta04909a**.

Acknowledgements

This work was performed in the cooperation framework of Wetsus, European Centre of Excellence for Sustainable Water Technology (**https://www.wetsus.nl/**). Wetsus is co-funded by the European Union (Horizon Europe, LIFE, Interreg and EDRF), the Province of Fryslân and the Dutch Government: Ministry of Economic Affairs (TTT, SBO & PPS-I/TKI Water Technology), Ministry of Education, Culture and Science (TTT & SBO) and Ministry of Infrastructure and Water Management (National Growth Fund - UPPWATER). The project leading to this publication has received funding from the European Union's Horizon 2020 research and innovation programme under grant agreement no. 101022484. The authors like to thank the participants of the research theme "Sustainable carbon cycle" for the fruitful discussions and their financial support.

References

1 *Copernicus: 2023 is the hottest year on record, with global temperatures close to the 1.5 °C limit*, 2023, **https://climate.copernicus.eu/copernicus-2023-hottest-year-record**, accessed January 2025.

2 V. Masson-Delmotte, P. Zhai, H.-O. Pörtner, D. Roberts, J. Skea, P. R. Shukla, A. Pirani, W. Moufouma-Okia, C. Péan, R. Pidcock, S. Connors, J. B. R. Matthews, Y. Chen, X. Zhou, M. I. Gomis, E. Lonnoy, T. Maycock, M. Tignor and T. Waterfield, in *Global Warming of 1.5°C*, Cambridge University Press, 2022, pp. 3–24.

3 M. D. Eisaman, L. Alvarado, D. Larner, P. Wang, B. Garg and K. A. Littau, CO_2 separation using bipolar membrane electrodialysis, *Energy Environ. Sci.*, 2011, **4**, 1319–1328, DOI: **10.1039/C0EE00303D**.

4 M. Bui, C. S. Adjiman, A. Bardow, E. J. Anthony, A. Boston, S. Brown, P. S. Fennell, S. Fuss, A. Galindo, L. A. Hackett, J. P. Hallett, H. J. Herzog, G. Jackson, J. Kemper, S. Krevor, G. C. Maitland, M. Matuszewski, I. S. Metcalfe, C. Petit, G. Puxty, J. Reimer, D. M. Reiner, E. S. Rubin, S. A. Scott, N. Shah, B. Smit, J. P. M. Trusler, P. Webley, J. Wilcox and N. Mac Dowell, Carbon capture and storage (CCS): the way forward, *R. Soc. Chem.*, 2018, **11**, 1062–1176, DOI: **10.1039/c7ee02342a**.

5 T. Moeller, J. C. Bailar, J. Kleinberg, C. O. Guss, M. E. Castellion and C. Metz, in *Chemistry*, ed. T. Moeller, J. C. Bailar, J. Kleinberg, C. O. Guss, M. E. Castellion and C. Metz, Academic Press, 1980, pp. 744–764.

6 S. Jin, M. Wu, Y. Jing, R. G. Gordon and M. J. Aziz, Low energy carbon capture via electrochemically induced pH swing with electrochemical rebalancing, *Nat. Commun.*, 2022, **13**, DOI: **10.1038/s41467-022-29791-7**.

7 M. C. Stern and T. Alan Hatton, Bench-scale demonstration of CO_2 capture with electrochemically-mediated amine regeneration, *RSC Adv.*, 2014, **4**, 5906–5914, DOI: **10.1039/C3RA46774K**.

8 M. Wang, H. J. Herzog and T. A. Hatton, Improved CO_2 Capture Performance of Electrochemically Mediated Amine Regeneration Processes with Ionic Surfactant Additives, *Ind. Eng. Chem. Res.*, 2020, **59**, 7087–7096, DOI: **10.1021/acsaem.0c01859**.

9 Q. Shu, L. Legrand, P. Kuntke, M. Tedesco and H. V. M. Hamelers, Electrochemical Regeneration of Spent Alkaline Absorbent from Direct Air Capture, *Environ. Sci. Technol.*, 2020, **54**, 8990–8998, DOI: **10.1021/acs.est.0c01977**.

10 F. Sabatino, M. Mehta, A. Grimm, M. Gazzani, F. Gallucci, G. J. Kramer and M. van Sint Annaland, Evaluation of a Direct Air Capture Process Combining Wet Scrubbing and Bipolar Membrane Electrodialysis, *Ind. Eng. Chem. Res.*, 2020, **59**(15), 7007–7020, DOI: **10.1021/acs.iecr.9b05641**.

11 A. Iizuka, K. Hashimoto, H. Nagasawa, K. Kumagai, Y. Yanagisawa and A. Yamasaki, Carbon dioxide recovery from carbonate solutions using bipolar membrane electrodialysis, *Sep. Purif. Technol.*, 2012, **101**, 49–59, DOI: **10.1016/j.seppur.2012.09.016**.

12 H. Nagasawa, A. Yamasaki, A. Iizuka, K. Kumagai and Y. Yanagisawa, A new recovery process of carbon dioxide from alkaline carbonate solution via electrodialysis, *AIChE J.*, 2009, **55**(12), 3286–3293, DOI: **10.1002/aic.11907**.

13 J. C. Bui, É. Lucas, E. W. Lees, A. K. Liu, H. A. Atwater, C. Xiang, A. T. Bell and A. Z. Weber, Analysis of bipolar membranes for electrochemical CO_2 capture from air and oceanwater, *Energy Environ. Sci.*, 2023, **16**, 5076–5095, DOI: **10.1039/D3EE01606D**.

14 R. Sharifian, R. M. Wagterveld, I. A. Digdaya, C. Xiang and D. A. Vermaas, Electrochemical carbon dioxide capture to close the carbon cycle, *R. Soc. Chem.*, 2021, **14**, 781–814, DOI: **10.1039/d0ee03382k**.

15 F. Bisotti, K. A. Hoff, A. Mathisen and J. Hovland, Direct Air capture (DAC) deployment: A review of the industrial deployment, *Chem. Eng. Sci.*, 2024, **283**, 119416, DOI: **10.1016/j.ces.2023.119416**.

16 S. Vallejo Castaño, Q. Shu, M. Shi, R. Blauw, P. Loldrup Fosbøl, P. Kuntke, M. Tedesco and H. V. M. Hamelers, Optimizing alkaline solvent regeneration through bipolar membrane electrodialysis for carbon capture, *Chem. Eng. J.*, 2024, **488**, 150870, DOI: **10.1016/j.cej.2024.150870**.

17 M. Shi, S. Vallejo Castaño, Q. Shu, M. Tedesco, P. Kuntke, H. V. M. Hamelers and P. Loldrup Fosbøl, Carbon capture via electrochemically mediated alkaline absorption: Lab-scale continuous operation, *J. Cleaner Prod.*, 2024, **476**, 143767, DOI: **10.1016/j.jclepro.2024.143767**.

18 R. Pärnamäe, M. Tedesco, M. C. Wu, C. H. Hou, H. V. M. Hamelers, S. K. Patel, M. Elimelech, P. M. Biesheuvel and S. Porada, Origin of Limiting and Overlimiting Currents in Bipolar Membranes, *Environ. Sci. Technol.*, 2023, **57**(26), 9664–9674, DOI: **10.1021/acs.est.2c09410**.

19 M. A. Blommaert, J. A. H. Verdonk, H. C. B. Blommaert, W. A. Smith and D. A. Vermaas, Reduced Ion Crossover in Bipolar Membrane Electrolysis *via* Increased Current Density, Molecular Size, and Valence, *ACS Appl. Energy Mater.*, 2020, **3**, 5804–5812, DOI: **10.1021/acsaem.0c00687**.

20 B. Bauer, F. J. Gerner and H. Strathmann, Development of Bipolar Membranes, *Desalination*, 1988, **68**, 279–292, DOI: **10.1016/0011-9164(88)80061-4**.

21 N. Wang, D. Wang, A. Krook-Riekkola and X. Ji, MEA-based CO_2 capture: a study focuses on MEA concentrations and process parameters, *Front. Energy Res.*, 2023, **11**, DOI: **10.3389/fenrg.2023.1230743**.

22 S. H. B. Vinjarapu, R. Neerup, A. H. Larsen, J. K. Jørsboe, S. N. B. Villadsen, S. Jensen, J. L. Karlsson, J. Kappel, H. Lassen, P. Blinksbjerg, N. von Solms and P. L. Fosbøl, Results from pilot-scale CO capture testing using 30 wt% MEA at a Waste-to-Energy facility: optimisation through parametric analysis, *Appl. Energy*, 2024, **355**, 122193, DOI: **10.1016/j.apenergy.2023.122193**.

23 Y. A. Çengel, M. A. Boles and M. Kanoğlu, *Thermodynamics: An Engineering Approach*, McGraw-Hill, 2020, p. 942.

24 P. Zhu, Z. Y. Wu, A. Elgazzar, C. Dong, T. U. Wi, F. Y. Chen, Y. Xia, Y. Feng, M. Shakouri, J. Y. (Timothy) Kim, Z. Fang, T. A. Hatton and H. Wang, Continuous carbon capture in an electrochemical solid-electrolyte reactor, *Nature*, 2023, **618**, 959–966, DOI: **10.1038/s41586-023-06060-1**.

25 E. Al-Dhubhani, R. Pärnamäe, J. W. Post, M. Saakes and M. Tedesco, Performance of five commercial bipolar membranes under forward and reverse bias conditions for acid-base flow battery applications, *J. Membr. Sci.*, 2021, **640**, 119748, DOI: **10.1016/j.memsci.2021.119748**.